Available online at BCREC website: https://bcrec.id

Bulletin of Chemical Reaction Engineering & Catalysis, 18 (3) 2023, 485-498

Research Article

Carbon Microspheres with Cr (VI) Adsorption Performance were Prepared by In-situ Hydrothermal Carbonization Method

Shaojie Chen[1], Xinzhuo Wu[1,2], Mei Li[1], Yuhan Xu[1], Zihao Yuan[1], Zhao Li[1], Jing Li[1,2,*]

[1]*School of Materials and Chemical Engineering, Xuzhou University of Technology, 221018, Xuzhou, China.*
[2]*School of Chemistry and Environmental Science, Yili Normal University, 835000, Yining, China.*

Received: 24th August 2023; Revised: 29th September 2023; Accepted: 30th September 2023
Available online: 2nd October 2023; Published regularly: October 2023

Abstract

Biochar material is a renewable adsorbent widely used for treating contaminated wastewater. The hydrothermal carbon (HTC) were prepared from low polymeric sugars and low concentration glucose under hydrothermal carbonization reactions without using dispersants. The composition and structure of the biochar produced were characterized using X-ray diffraction (XRD), Fourier transform infrared spectroscopy (FTIR), scanning electron microscopy (SEM), Raman spectroscopy (Raman), and N_2 adsorption-desorption, indicating that amorphous graphitic carbon was obtained. Experimental results from the static adsorption of Cr(VI)-contaminated wastewater showed that HTCP-2 exhibited the highest adsorption capacity for Cr(VI), with a maximum adsorption capacity of 22.62 $mg.g^{-1}$.The adsorption Cr(VI), MB, and RhB by the synthesized biochar all conformed to the pseudo-second-order kinetic model and Freundlich isotherm, suggesting a multilayer chemical adsorption process. Additionally, the synthesized HTC surface is enriched with a significant amount of oxygen-rich functional groups, which also has good adsorption performance for cationic dyes. Furthermore, the test results of fluorescence, photocurrent, and impedance indicate that HTCP-2 possesses the ability to generate and separate photoinduced charge carriers. This implied that HTCP-2 can be used for the preparation of adsorption photocatalysts, which effectively remove environmental pollutants through the synergistic effect of adsorption-photocatalysis. This study provides a research foundation for advancing water treatment technologies.

Keywords: Hydrothermal carbonization; Low polymerization sugar; Adsorption removal; Hexavalent chromium; Renewable

How to Cite: S. Chen, X. Wu, M. Li, Y. Xu, Z. Yuan, Z. Li, J. Li (2023). Carbon Microspheres with Cr (VI) Adsorption Performance were Prepared by In-situ Hydrothermal Carbonization Method. *Bulletin of Chemical Reaction Engineering & Catalysis*, 18(3), 485-498 (doi: 10.9767/bcrec.20026)

Permalink/DOI: https://doi.org/10.9767/bcrec.20026

1. Introduction

Wastewater containing Cr(VI) from industries such as electroplating, metallurgy, and leather production is characterized by its high toxicity, carcinogenicity, and mobility in water. Moreover, Cr(VI) can accumulate in organisms and can not be naturally photodegraded, making it a prioritized pollutant for global control [1–7]. Currently, the technologies for treating Cr(VI)-contaminated wastewater include adsorption [1,2], ion exchange [3], membrane separation [4], chemical reduction [5], and photocatalytic reduction [6]. The adsorption method, commonly used for the treatment of Cr(VI)-contaminated wastewater [1,2,7–10], has the advantages of high selectivity, low energy con-

* Corresponding Author.
Email: lijingxz111@163.com (J. Li);
Phone: +86 15950689529, Fax: +86 0516-85608369

sumption, minimal by-products, and strong adsorption capacity. Meanwhile, adsorbents, such as Mn-incorporated ferrihydrite [1], montmorillonite nanocomposites [2], biochar [9], silicas [10], and so on, adsorb Cr(VI) to the active sites through mechanisms such as adsorption, chelation, or ion exchange. Furthermore, the purification of Cr(VI)-contaminated wastewater can be achieved by utilizing adsorption or the synergistic effect of adsorption combined with photocatalysis. Due to the close correlation between the effectiveness of adsorption in eliminating environmental pollutants and the type of adsorbent used, the development of high-performance adsorbents is of significant importance for the treatment of environmental wastewater.

Biomass can be pyrolyzed under anaerobic or oxygen-limited conditions to obtain carbon-rich, highly aromatic, and porous solid biochar materials [11], which possess abundant pore structures, a large specific surface area, and rich oxygen-containing functional groups on their surface. Biochar materials also exhibit excellent optical, electrical, mechanical, and chemical properties, finding wide applications in the fields of environment and energy [11–15]. The methods for preparing biochar materials include the template method [11], chemical vapor deposition (CVD) [12], high-temperature pyrolysis [13], and hydrothermal carbonization [14–16]. Among them, hydrothermal carbonization is an exothermic reaction in which carbohydrates are used as raw materials and water serves as the reaction medium. This reaction takes place at certain solid-liquid ratios, temperatures (100–250 °C), reaction times (4–24 h) and (0.5–16.5 MPa), with the solid products as the target products [14–19]. Hydrothermal carbonization technology offers advantages such as low raw material costs, low energy consumption, simple operation, a high conversion rate, and controllable preparation of carbon materials [17–20]. Hydrothermal carbonization technology differs fundamentally from the combustion process that releases CO_2 and can effectively reduce CO_2 greenhouse gas emissions. In this regard, hydrothermal carbonization is considered a promising technology for the production of biochar materials.

The synthetic method of producing carbon materials using biomass as raw materials aligns with the trends of economic, low-energy consumption, and environmentally sustainable development. Various natural substances, such as sugars (glucose, fructose, trehalose, xylan, *etc.*), lignin, cellulose, biomass waste, *etc.* [17–27], can be used to prepare hydrothermal carbon and serve as adsorbents for the adsorption treatment of U(VI) [18], Cr(VI) [1,2,17,21,22], copper ions [25], methylene blue [19,25], blue 41 [13], RhB [24], iodine [25], nitrate [12], and CO_2 [20].

It has been shown that carbon microspheres are the main product of hydrothermal carbonization of sugars [11,28], which is a complex chemical process involving reactions such as dehydration, condensation, polymerization, and aromatization [26–29]. Considering the relationship between material structure and properties, the synthesis of carbon materials with excellent performance can be controlled through morphology control, performance modification, and analysis of hydrothermal carbonization mechanisms [14,28–32]. Ischia [28] utilized the hydrothermal carbonization reaction of glucose to study the reaction pathways and kinetics. He *et al.* [14] systematically investigated the reaction pathways and kinetics of the hydrothermal carbonization of glucose at 180℃, determining the structures of intermediates and the final chemical product. Their studies confirmed that 5-hydroxymethylfurfural (HMF) is the dominant intermediate product and the sole precursor of hydrothermal carbon, and they calculated the conversion rate of glucose and the yield of hydrothermal carbon. Also, the influence of reaction temperature on the shape and size of hydrothermal carbon was analyzed. Sun *et al.* [17] prepared porous carbon microspheres through a two-step method involving hydrothermal carbonization and KOH or NH_3 activation. Experimental results showed that the Cr(VI) adsorption by porous carbon microspheres followed Langmuir monolayer adsorption. Yao *et al.* [30] employed sulfuric acid-catalyzed hydrothermal carbonization to prepare glucose-based porous carbon materials while achieving improved yield. The resulting mesoporous materials with negatively surfaces charged exhibited optimal adsorption performance for methylene blue (MB). Jung *et al.* [26] investigated the effect of salt additives (KCl and $CaCl_2$) and reactor stirring on the preparation of carbon spheres through fructose hydrothermal carbonization. The study revealed that the addition of salts enhanced the reaction rate without altering the size of the products. Li *et al.* [31] utilized the glucose hydrothermal method to prepare carbon microspheres with regular shapes and abundant oxygen functional groups. The reaction temperature (180–270 °C) influenced the chemical properties and morphology of the carbon microspheres. Increasing the glucose concentration

(0.3–0.7 M) resulted in larger carbon spheres, while the morphology of the carbon spheres remained unaffected. The above findings contribute to the advancement of hydrothermal carbonization technology. However, the reaction of hydrothermal preparation of biochar is uncontrollable and complex, and the reaction pathways and kinetics may differ for various sugar hydrothermal carbonization processes. In the existing studies, the performance of biochar prepared from low-polymerized sugars has not been thoroughly and systematically investigated. The use of dispersants or morphology controllers leads to higher raw material input costs and complex synthesis routes. In addition, higher reaction temperatures not only increase energy consumption, but also lead to the reduction of functional groups on the surface of biochar.

From the perspective of environmental sustainability, the utilization of biomass feedstock for the preparation of hydrothermal carbon holds great potential. According to the aforementioned analysis, this study aims to investigate the composition and structure of hydrothermal carbonization products derived from low-concentration glucose solutions and low-polymerization sugars without the use of dispersants and morphology-controlling agents. The synthesis mechanism of HTC by the low-temperature hydrothermal method was proposed according to the characterization analysis of HTC composition and structure. Systematically investigated the kinetic and thermodynamic characteristics of HTC adsorbed pollutants, as well as the selectivity using Cr(VI) and organic dye pollutants as simulations of pollutants. The photoelectric properties of HTC were investigated, that providing significant potential for the synergistic treatment of pollutants through adsorption-photocatalysis.

2. Materials and Methods

2.1 Synthesis of Carbon Microspheres

Accurately weighed 1.4400 g, 2.8800 g, and 4.3200 g of glucose, dissolved them in 80.00 mL of deionized water, and magnetically stirred for 20 min to obtain a glucose aqueous solution. Further, the above solution was transferred to a stainless steel autoclave lined with polytetrafluoroethylene reactor at 180 °C for 12 h. After the reaction is complete, cool naturally to room temperature, then wash with deionized water. The obtained brown product is dried in a 100 °C oven for 4 h. The dried samples are ground to obtain carbon microsphere powder. The obtained samples prepared with low to high glucose concentrations were named HTCP-1, HTCP-2 and HTCP-3, respectively. The carbon microspheres labeled HTCR, HTCZ, and HTCK were obtained by the same synthesis route using a 0.2 mol.L^{-1} solution of lactose, sucrose, and chitosan, respectively.

2.2 Characterizations of HTC

The crystallinity of the synthesized HTC was analyzed by the Rigaku Corporation Ultima IV X-ray powder diffractometer using Cu target Kα radiations (λ = 0.1541 nm) and incident angle range of 10–80°. The compositional and structural characterization has been carried out on a Renishaw Invia Raman spectrometer and a Bruker ALPHA FTIR spectrometer. The morphologies of the samples were observed by a Hitachi SU8600 field-emission scanning electron microscope (FESEM), and the accelerating voltage of the test was 10 kV. The specific surface area of the HTC was measured by the ASAP 2460 Multi-station Automatic Specific Surface Area and Pore Size Analyzer. The materials were treated under a nitrogen atmosphere at 200 ℃ for 12 h before testing, and the experimental results were analyzed by the BJH model, which was used to calculate the pore size distribution of the HTC. The diffuse reflection spectrum was obtained by UV-vis diffuse reflectance absorption spectroscopy (UV-vis DRS) of PELambda750, USA, $BaSO_4$ was used as the blank substrate, and the spectral scanning range was 250–800 nm. The Shanghai Chenhua CHI660E electrochemical workstation was used to test the photocurrent (i–t) and electrochemical impedance (EIS) of the samples, and the three-electrode system was used for the test, with Pt as the auxiliary electrode and Ag/AgCl as the reference electrode.

2.3 Adsorption Experiment (Adsorption Capacity and Removal Rate)

The experiments of Cr(VI) adsorption by the prepared HTC were conducted under light avoidance conditions at room temperature of 25 ℃, while the rate of magnetic stirring was a fixed 460 rpm and the stirring was lasting for 18 h. Aqueous Cr(VI) with concentrations ranging from 10 to 100 mg.L^{-1} (10, 20, 30, 40, 60, 80, and 100 mg.L^{-1}, pH 6) was prepared, and the dosage of HTC was 1 g.L^{-1}. After a specified reaction time, 4 mL of the reaction solution is taken from the reaction system and separated by centrifugation to obtain a clear solution of adsorbed Cr(VI). The concentration of Cr(VI) is then measured using the diphenylcarbazide spectrophotometric method at 540 nm.

To investigate the effect of pH on the adsorption performance of Cr(VI) by HTCP-2, 30 mg·L^{-1} of Cr(VI) was used as a simulated pollutant, and the pH of the Cr(VI) solution was regulated to be 2, 3, 4, 6, and 8 with 0.2 M H_2SO_4 and 0.2 M NaOH, and the same stirring rate and adsorption time were maintained. The concentration of Cr(VI) in the solution was detected using the above method. The adsorption selectivity of HTCP-2 was investigated using the same experimental method. The pH value of solution was 6, the same stirring rate and adsorption time were maintained by utilizing a solution containing 10 mg.L^{-1} methylene blue (MB), Rhodamine B (RhB) and Cr(VI) as contaminants, respectively. The concentrations of MB and RhB after adsorption were measured by a UV – vis spectrophotometer at 664 nm and 554 nm.

Equation (1) [1,2] was used to calculate the adsorption removal rate of Cr(VI) by carbon microspheres. Furthermore, the equilibrium adsorption capacity of HTCP-2 for Cr(VI) was calculated using Equation (2) [33,34]. Adsorption kinetics. Fitting the adsorption behavior of hexavalent chromium on HTC using pseudo-first-order kinetic and pseudo-second-order kinetic models (Equations (3) and (4) [33,34]). The Langmuir adsorption isotherm equation (Equation (5) [34–36]) and the Freundlich adsorption isotherm equation (Equation (6) [21,30]) were used to describe the monolayer or multilayer adsorption process on the surface of HTC.

Adsorption removal rate [33,34]:

$$R(\%) = \frac{c_0 - c_t}{c_0} \times 100\% \quad (1)$$

Adsorption capacity [33,34]:

$$Q_e = \frac{(c_0 - c_e) \times V}{m} \quad (2)$$

Pseudo-first-order kinetic model [33,34]:

$$\ln(Q_e - Q_t) = \ln Q_e - k_1 t \quad (3)$$

Pseudo-second-order kinetic model [33,34]:

$$\frac{t}{Q_t} = \frac{1}{k_2 Q_e^2} + \frac{t}{Q_e} \quad (4)$$

Langmuir model [21,30,34–36]:

$$Q_e = \frac{Q_{\max} k_L c_e}{1 + k_L c_e} \quad (5)$$

Freundlich model [21,30]:

$$Q_e = k_F c_e^{-n} \quad (6)$$

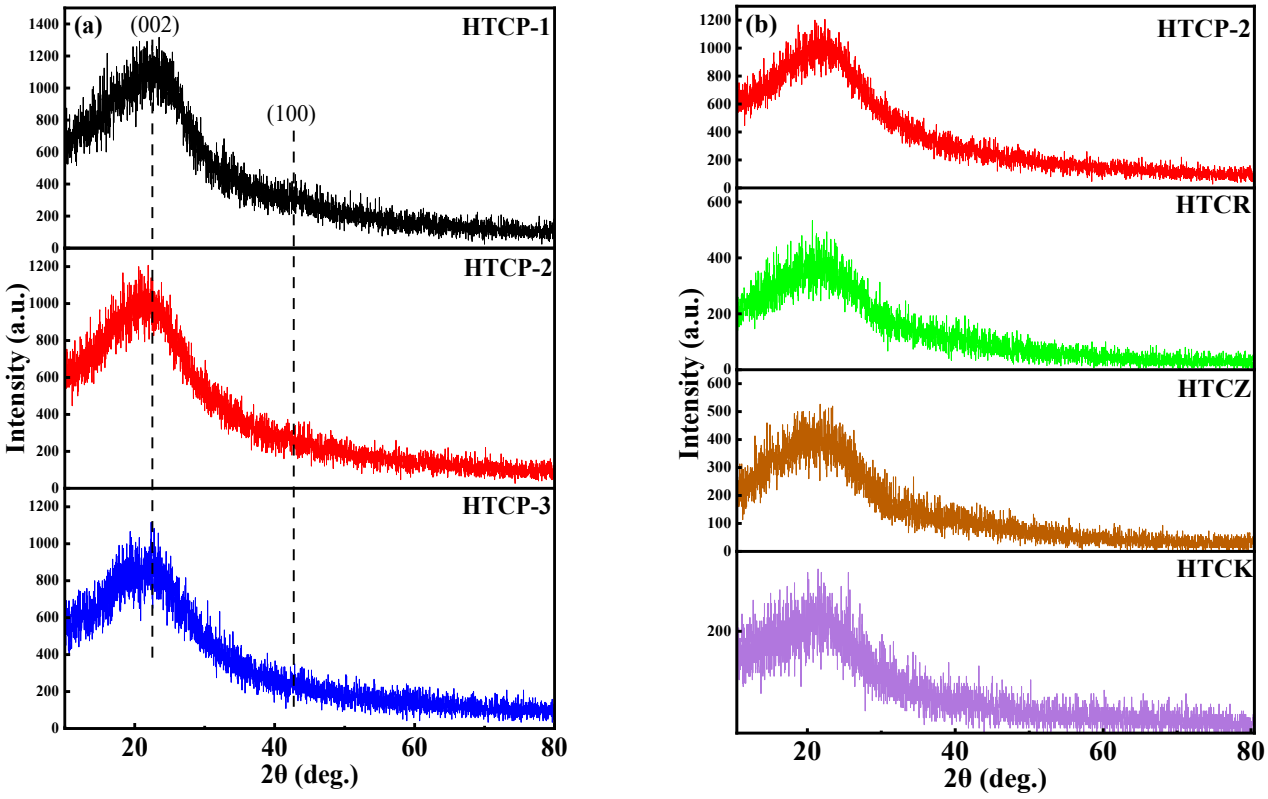

Figure 1. XRD patterns of as-synthesized HTC, (a) HTCP-1, HTCP-2, and HTCP-3, (b) HTCR, HTCZ, and HTCK.

where, Q_e represents the equilibrium adsorption capacity (mg.g^{-1}), c_0, c_t, and c_e are the initial concentration, concentration at time t, and equilibrium concentration of Cr(VI) aqueous solution (mg.L^{-1}), respectively, m is the mass of the adsorbent (mg), V is the volume of the solution (L), and k_L and k_F represent the Langmuir and Freundlich constants, respectively.

3. Results and Discussion

3.1. Structure and Composition

The XRD patterns of carbon microspheres prepared by hydrothermal carbonization with different sugars as raw materials were provided in Figure 1. The similar shape of the diffraction peaks of the as-synthesized HTCP-1, HTCP-2, HTCP-3, HTCR, HTCZ, and HTCK, suggesting the formation of similar compositions of the products. The XRD patterns of HTCP-1, HTCP-2, and HTCP-3, shown in Figure 1(a), are hydrothermal carbonization products obtained from different glucose concentrations as starting materials. The diffraction peak at 2θ angles of 22.6° corresponded to the (002) plane of graphite carbon. The broadness of the diffraction peak indicated the formation of amorphous graphitized carbon material. The weak diffraction peaks exist at 42.8° in Figure 1, corresponding to the plane (100) of graphite [27,31,32]. The XRD pattern results revealed that as the concentration of glucose solution increases, the intensity of XRD diffraction peaks of glucose-derived carbon spheres decreases, indicating a decrease in the degree of graphitization of the produced carbon material. Figure 1(b) showed the XRD patterns of HTCR, HTCZ, and HTCK obtained by hydrothermal carbonization prepared from sucrose, lactose, and chitosan, which showed weaker intensity of XRD diffraction peaks than that of HTCP. This is possibly due to the hydrothermal carbonization process using disaccharides and polysaccharides as raw materials, which involves the initial hydrolysis to form monosaccharides. The hydrolysis process consumes energy and affects the formation of hydrothermal carbon.

The chemical bonds of the synthesized char materials were analyzed by Fourier transform infrared (FTIR) spectroscopy (Figure 2(a)). The prepared hydrothermal carbon materials had similar infrared profiles. The absorption peak at 795 cm^{-1} can be ascribed to the out-of-plane bending vibration of C−H in the RCH=CHR groups [21,27]. The bands at 1194 cm^{-1} and 1020 cm^{-1} were assigned to the C−O stretching vibration [24,32]. The band at 1299 cm^{-1} corresponded to the deformation vibration of O−H. The characteristic peaks at 1606 cm^{-1} and 1492 cm^{-1} are associated with the vibration of C=C bonds [30,32]. The absorption peak at 1710 cm^{-1} indicated the presence of C=O stretching vibration on the surface of the material. The peak that appeared at 2921 cm^{-1} could be ascribed to the stretching vibration of aliphatic C−H bonds. The characteristic broadband near 3415 cm^{-1} was attributed to the stretching vibration of O−H originating from the residual water or acid, indicating the presence of crystalline water on the sample surface, which was caused by moisture absorption after drying.

Further, the graphite-like structure of HTCP-2 was revealed by Raman spectroscopy [21]. There were two distinct absorption peaks in the Raman spectrum due to defect structure and graphitization structures (Figure 2(b)). The G band at 1576 cm^{-1} was related to the in-plane vibration of the sp^2 bonded crystallite carbon, while another peak at 1362 cm^{-1} of the D band is attributed to defect sites or disor-

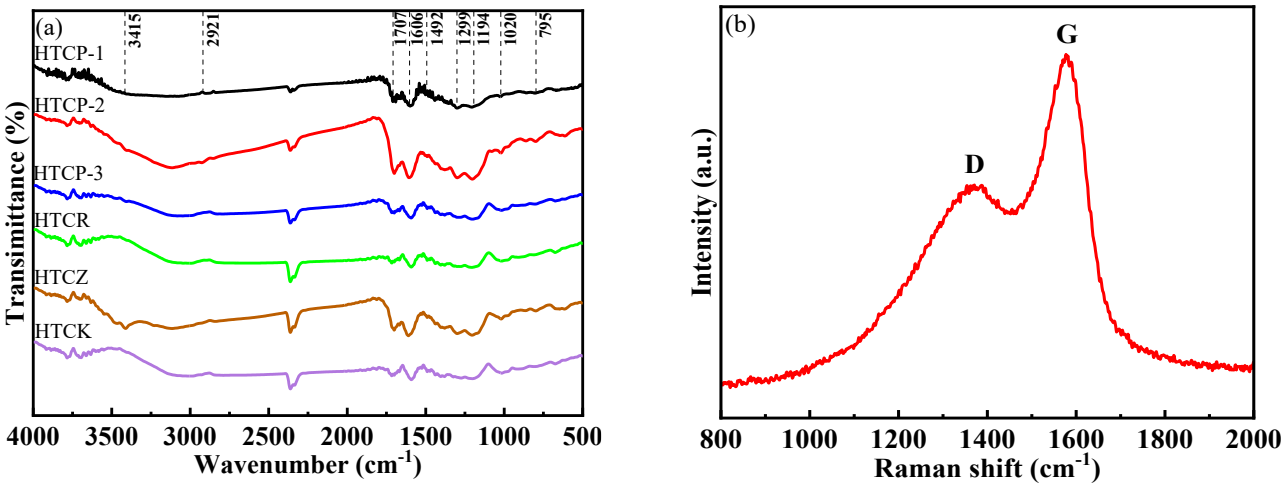

Figure 2. (a) FTIR spectra of HTCP, HTCR, HTCZ, and HTCK, (b) Raman spectroscopy of HTCP-2.

dered carbon formation. The experimental results suggested that the surface of hydrothermally carbonized microspheres typically contains abundant functional groups, and the type and concentration of sugars used as synthetic raw materials do not impact the composition of the hydrothermal carbon.

3.2 Morphologies and Synthesis Mechanism

The morphology of HTC synthesized without dispersant was shown in Figure 3. HTC consists of microspheres with diameters ranging from 4.5 to 6.5 μm, as well as different numbers of oxygen-rich nanoclusters can be observed [27]. Figure 3(a), (b), and (c) showed the morphology of HTCP-1, HTCP-2, and HTCP-3 synthesized at concentrations of 0.1 M, 0.2 M, and 0.3 M, respectively, using glucose as a carbon source. Both HTCP-1 and HTCP-2 exhibited good dispersion. As the reactant concentration increases, the degree of aggregation and carbonization of the synthesized hydrothermal carbon decreases. The carbon microspheres of

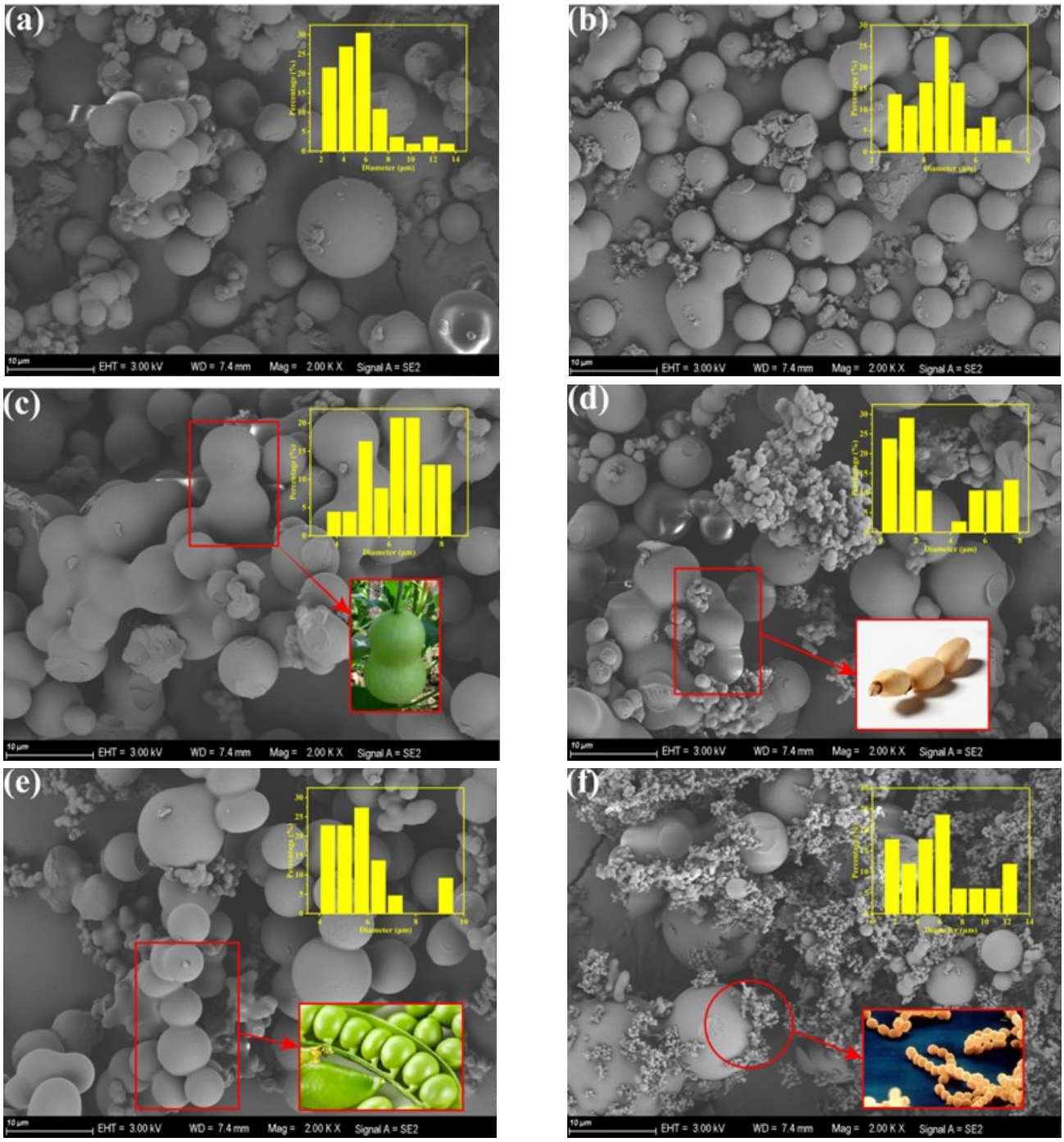

Figure 3. FESEM images of (a) HTCP-1, (b) HTCP-2, (c) HTCP-3, (d) HTCR, (e) HTCZ, and (f) HTCK.

HTCP-2 had the smallest size, while HTCP-3 consisted of gourd-shaped microspheres and monodisperse microspheres.

Figure 3(d), (e), and (f) showed the microscopic morphology of HTCR, HTCZ and HTCK prepared with lactose, sucrose and chitosan as carbon sources, respectively, a decrease in the number of monodisperse carbon spheres can be observed. Figure 3(d) presented rosette-like carbon spheres, a pea pod-like morphology appeared in Figure 3(e), and Figure 3(f) showed the lowest number of dispersed monodispersed spheres and a large number of carbon nanoclusters. The morphology of the hydrothermal carbon spheres indicated that reducing the concentration of raw materials and using monosaccharides and disaccharides with low polymerization were more beneficial to obtain biochar spheres with uniform size and well-dispersion, resulting in materials with excellent performance.

Based on the analysis of the composition, structure, and morphology of hydrothermal carbon, a synthesis mechanism was proposed. Glucose is an important polyhydroxy aldehyde monosaccharide with a pyranose structure in nature. The synthesis of hydrothermal carbon using glucose can be carried out at relatively low reaction temperatures. Through intermolecular dehydration at 160 °C, glucose can undergo polymerization and carbonization at a reaction temperature of 170 °C to form carbon microspheres [11–13].

In the hydrothermal carbonization process of polysaccharides and disaccharides, hydrolysis of the sugars occurs first to generate glucose and fructose, and the resulting monosaccharides are converted into 5-hydroxymethylfurfural (HMF) through direct dehydration. Subsequently, HMF undergoes polymerization, condensation, and aromatization reactions to transform into hydrothermal carbon [12,14,28]. The hydrolysis reaction of polysaccharides consumes energy, thereby increasing the energy consumption of the reaction. The high surface energy of the reaction intermediates leads to the generation of oxygen-rich nanoclusters [27]. The synthesis mechanism of hydrothermal carbon is illustrated in Figure 4.

3.3 Adsorption Performance of Cr(VI) by HTC

3.3.1 N_2 adsorption-desorption isotherm

The surface structure and pore structures of HTCP-2, HTCR, and HTCZ were evaluated using the Brunauer-Emmett-Teller (BET) method (Figure 5) at 77 K and under the N_2 atmosphere. The N_2 adsorption-desorption isotherms of HTC exhibited a hysteresis loop in the range of relative pressures of 0.2–1.0. HTCP-2 exhibited a type IV-H3 adsorption-desorption isotherm (Figure 5(a)), and HTCZ and HTCR were classified as type IV-H4. The specific surface area of HTC was obtained using the Multi-Point BET method, and the pore volume and pore size distribution of each sample were also obtained. The BET-specific surface areas of HTCP-2, HTCR, and HTCZ were 64.31, 15.4923, and 2.04 $m^2.g^{-1}$, respectively, indicating that carbon microspheres possess mesoporous structures. The pore size of the three products are showed in the insert map of Figure 5, the test reports provided adsorption pore sizes of 3.418, 3.835, and 3.836 nm for HTCP-2, HTCR, and HTCZ, respectively, indicating that all of the materials obtained were mesoporous. The adsorption pore volume of the carbon microspheres was calculated using the BJH method, and the adsorption pore volumes of HTCP-2, HTCR, and HTCZ were found to be 0.310, 0.007, and 0.004 $cm^3.g^{-1}$. HTCP-2 has a largest adsorption pore volume and specific surface area, and therefore shows the best adsorption performance.

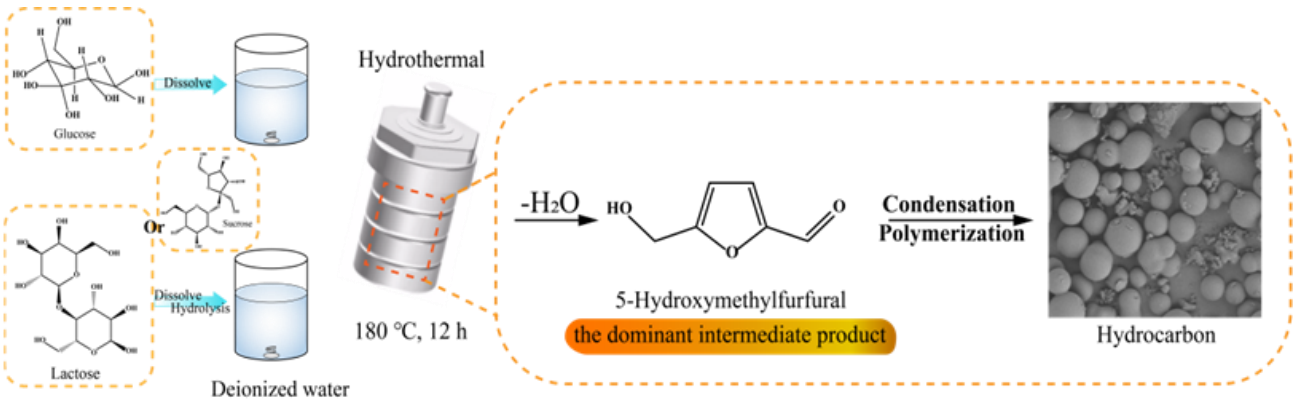

Figure 4. Synthesis of hydrothermal carbon.

3.3.2 Adsorption kinetics

The adsorption activity of HTCP-1, HTCP-2 and HTCP-3 were evaluated using 30 mg.L^{-1} Cr(VI) as a simulated pollutant. Figure 6(a) showed that the order of the instantaneous adsorption capacity of Cr(VI) is HTCP-1> HTCP-2> HTCP-3. The pseudo-first-order and pseudo-second-order kinetic models were used to analyze the adsorption of Cr(VI) by HTCP, and the correlation coefficients (R^2) of the fitted curves in Figure 6(b) and 6(c) showed that the R^2 value obtained from the pseudo-second-order kinetic model ($R^2 > 0.998$) was higher than that of the pseudo-first-order kinetic model ($R^2 < 0.948$). Therefore, adsorption of Cr(VI) by HTCP was more compatible with the pseudo-second-order kinetic model, indicating a chemical adsorption process. According to the pseu-

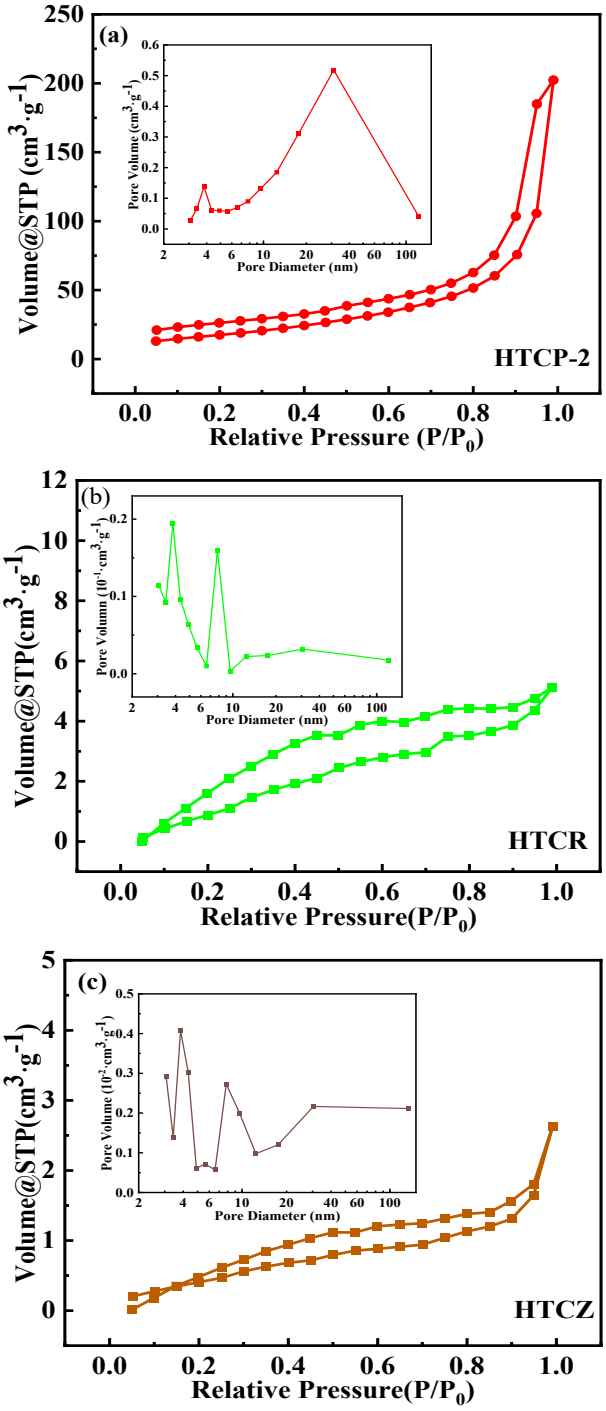

Figure 5. N_2 adsorption-desorption isotherms and pore-size distribution plots of (a) HTCP-2, (b) HTCR, and (c) HTCZ.

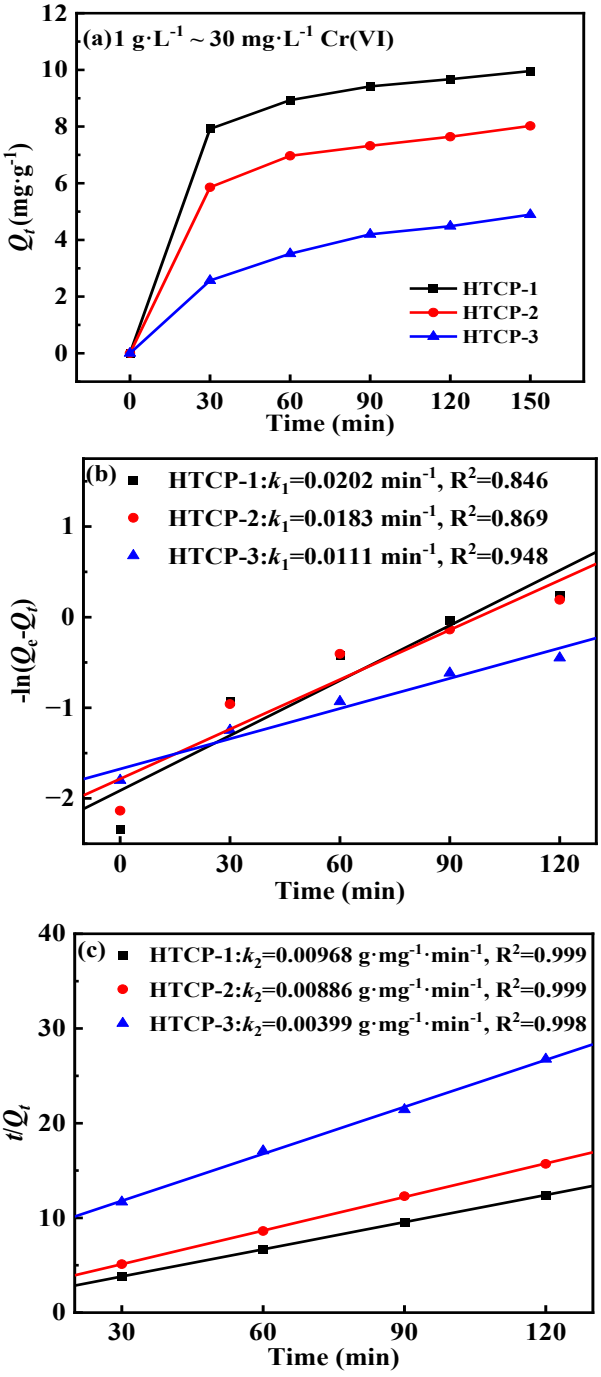

Figure 6. HTCP was prepared with glucose as a carbon source, (a) instantaneous adsorption amount, (b) pseudo-first-order kinetic model, and (c) pseudo-second-order kinetic model.

do-second-order kinetic model, the adsorption capacities HTCP-1, HTCP-2, and HTCP-3 for Cr(VI) were 10.45, 8.46, and 6.05 g.mg^{-1}, respectively, and the adsorption rates were 0.00968, 0.00886, and 0.00399 g.mg^{-1}.min^{-1}, respectively.

3.3.3 Adsorption isotherms of Cr(VI) on HTCP-2

As shown in Figure 7(a), the adsorption capacity of HTCP-2 for Cr(VI) increases with increasing Cr(VI) concentration. When the concentration of Cr(VI) is 80 mg.L^{-1}, the adsorption capacity of HTCP-2 for Cr(VI) is 22.62 mg.g^{-1}. However, when the concentration exceeds 80 mg.L^{-1}, the adsorption capacity gradually decreases with the increase in pollutant concentration, indicating that the adsorption of Cr(VI) by HTCP-2 is a chemical adsorption process, which is consistent with the results of kinetic fitting. In order to investigate the adsorption mechanism of HTCP-2 for Cr(VI), the Langmuir monolayer and Freundlich multilayer adsorption isotherm models (Equations (3) and (4)) were used to process the experimental data. The obtained adsorption isotherms are shown in Figure 7(b), compared to the Langmuir adsorption model, the Freundlich adsorption model has a greater non-linear fitting correlation coefficient R^2 (0.975 > 0.942). Therefore, the adsorption of Cr(VI) by HTCP-2 followed Freundlich multilayer adsorption. The effect of different pH value on Cr(VI) adsorption by HTCP-2 is shown in Figure 7(c). The adsorption capacity of HTCP-2 for Cr(VI) was greater at lower pH value than at higher pH value, and the adsorption capacity was maximum at pH 3, which indicated that the adsorption capacity of HTCP-2 for Cr(VI) was highly dependent on pH. This is due to the fact that at pH was 3, Cr(VI) compounds was present in the species of $HCrO_4^-$, which has good electrostatic attraction, so the adsorption capacity of biochar on Cr(VI) is better under acidic conditions. When pH >6, Cr(VI) compounds mainly existed as CrO_4^{2-}, the competition between CrO_4^{2-} and OH^- was more obvious, and the adsorption of Cr(VI) by biochar received inhibition [21].

3.3.4 Adsorption performance of hydrothermal carbon synthesized from disaccharides and polysaccharides for Cr(VI)

The adsorption performances of HTCP-2, HTCR, HTCZ, and HTCK for 30 mg.L^{-1} Cr(VI) were evaluated. Adsorption kinetics for Cr(VI) by the prepared hydrochars were shown in Figure 8(a), following the order HTCP-2 > HTCR > HTCZ > HTCK. Figure 8(b) and 8(c) demonstrated those the R^2 values of the pseudo-second-order kinetics of hydrothermal carbons

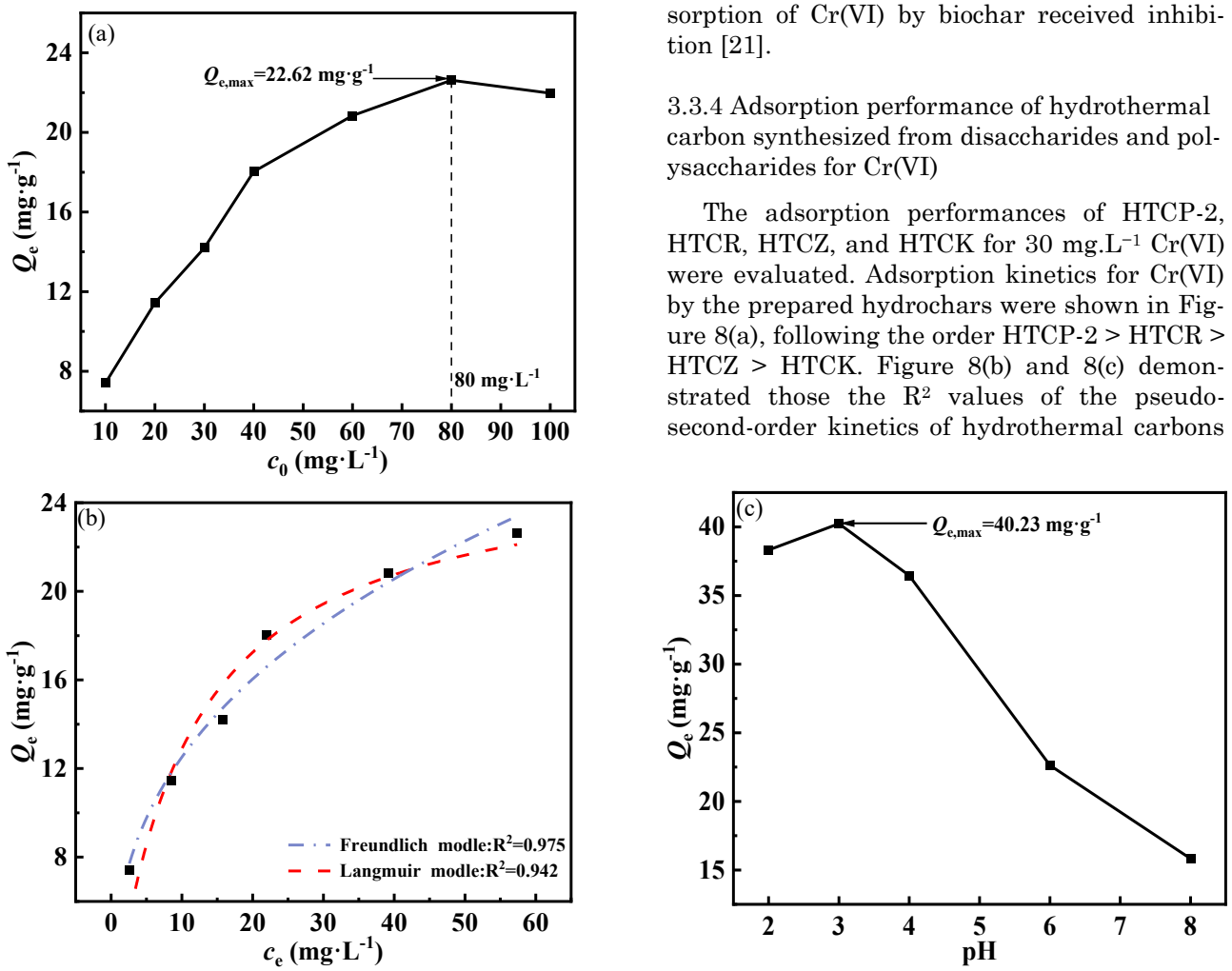

Figure 7. (a) Adsorption capacity of HTCP-2 for Cr(VI) (pH = 6), (b) adsorption isotherms of Cr(VI) on HTCP-2, (c) adsorption capacity of HTCP-2 for Cr(VI) under different solution pH (2~8).

for adsorbing Cr(VI) are higher than that of the pseudo-first-order kinetics, so the adsorption of Cr(VI) by the carbon microspheres synthesized from different sugars follows pseudo-second-order kinetics. The pseudo-second-order apparent kinetic rate constants of HTCP-2, HTCR, HTCZ, and HTCK for Cr(VI) adsorption, were determined to be 0.00886, 0.00766, 0.00580, and 0.00753 $g.mg^{-1}.min^{-1}$, respectively, with HTCP-2 exhibiting the highest adsorption rate. The characterization results of the composite materials indicate that the dispersion of the carbon microspheres has a significant positive influence on the adsorption effectiveness. Moreover, the adsorption capacities of HTCP-2, HTCR, HTCZ, and HTCK for 30 $mg.L^{-1}$ Cr(VI) were further obtained (Figure 8(d)), which were 8.46, 7.83, 6.26, and 7.24 $mg.g^{-1}$, respectively. Combined with the experimental results of N_2 adsorption-desorption tests, the adsorption removal capacity of the synthesized products for Cr(VI) was in the same order as the size of their specific surface area and pore volume. Among them, HTCP-2 has the largest specific surface area (64.31 $m^2.g^{-1}$) and adsorption pore volume (0.310 $cm^3.g^{-1}$). Among them, HTCP-2 has the largest specific surface area and pore volume, which has the optimal adsorption performance.

3.4 Adsorption Performance of MB and RhB Dye by HTCP-2

Figure 9(a) presents the performance of HTCP-2 in adsorbing 10 $mg.L^{-1}$ MB, RhB and Cr(VI), respectively, results of the adsorption experiments showed that the adsorption activity of HTCP-2 for pollutants followed the order MB > RhB > Cr(VI). The analysis of the kinetic models in Figure 9(b) and Figure 9(c) also indicated that the adsorption of dyes by HTCP-2 followed pseudo-second-order kinetics. Combined with the experimental results of infrared

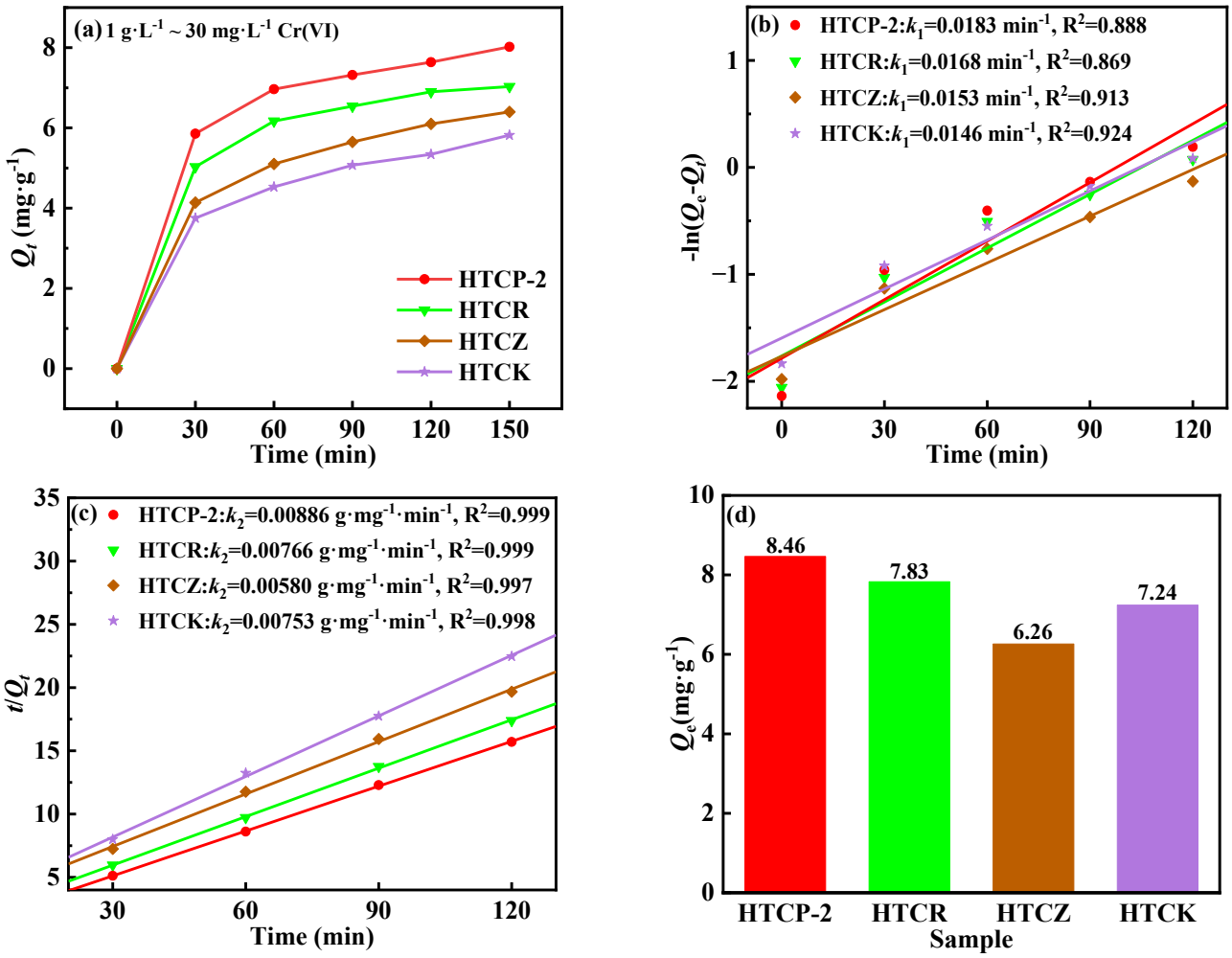

Figure 8. Adsorption characteristics of 30 $mg.L^{-1}$ Cr(VI) by HTCP-2, HTCR, HTCZ, and HTCK, (a) instantaneous adsorption amount, (b) pseudo-first-order kinetic model, (c) pseudo-second-order kinetic model, (d) equilibrium adsorption capacity.

and Raman spectroscopy, it is observed that the presence of abundant anionic functional groups such as O−H, C−O, and C=O on the surface of carbon microspheres, enhanced the electrostatic adsorption process for cationic dyes such as methylene blue and rhodamine. This explains the enhanced adsorption performance of the carbon microspheres for cationic dyes.

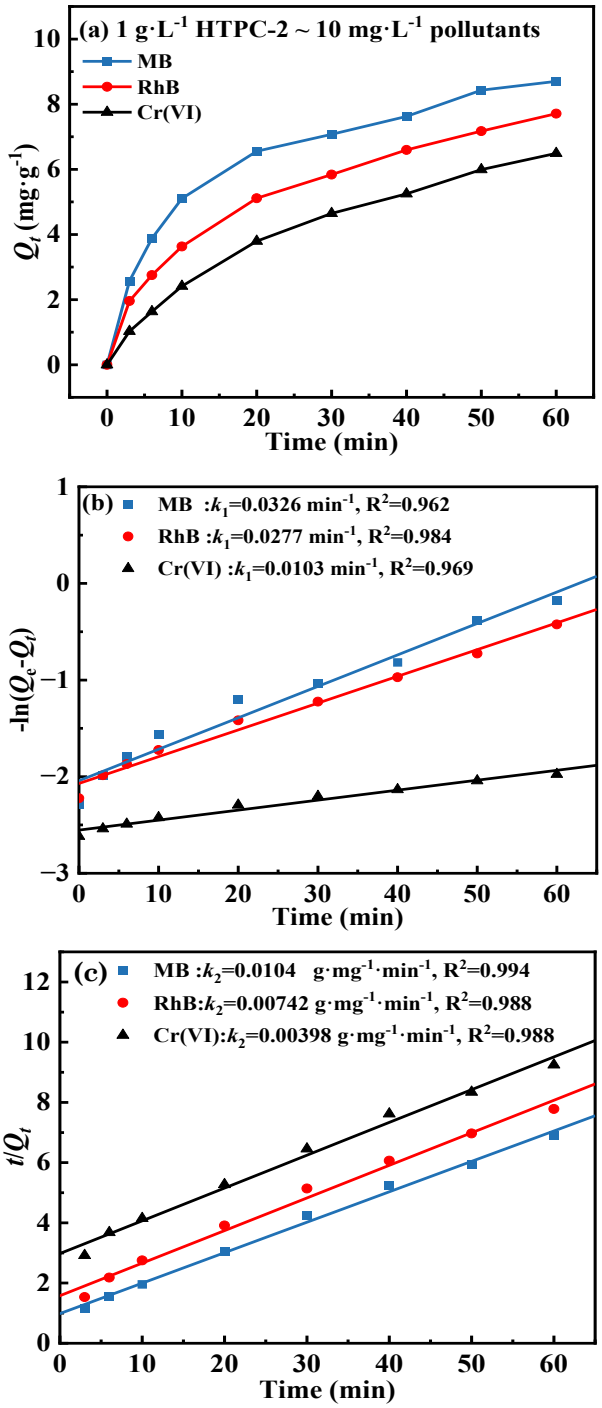

Figure 9. Adsorption characteristics of 10 mg.L^{-1} Cr(VI), MB, and RhB by HTCP-2, (a) instantaneous adsorption amount, (b) pseudo-first-order kinetic model, (c) pseudo-second-order kinetic model.

3.5 Optoelectronic Performance Analysis of HTCP-2

The photoluminescence (PL) performance of a material is the spontaneous emission of light under appropriate light excitation, which has applications in many fields such as bioimaging, LEDs, or catalysis [12].The fluorescence spectrum of HTCP-2 is shown in Figure 10(a), ex-

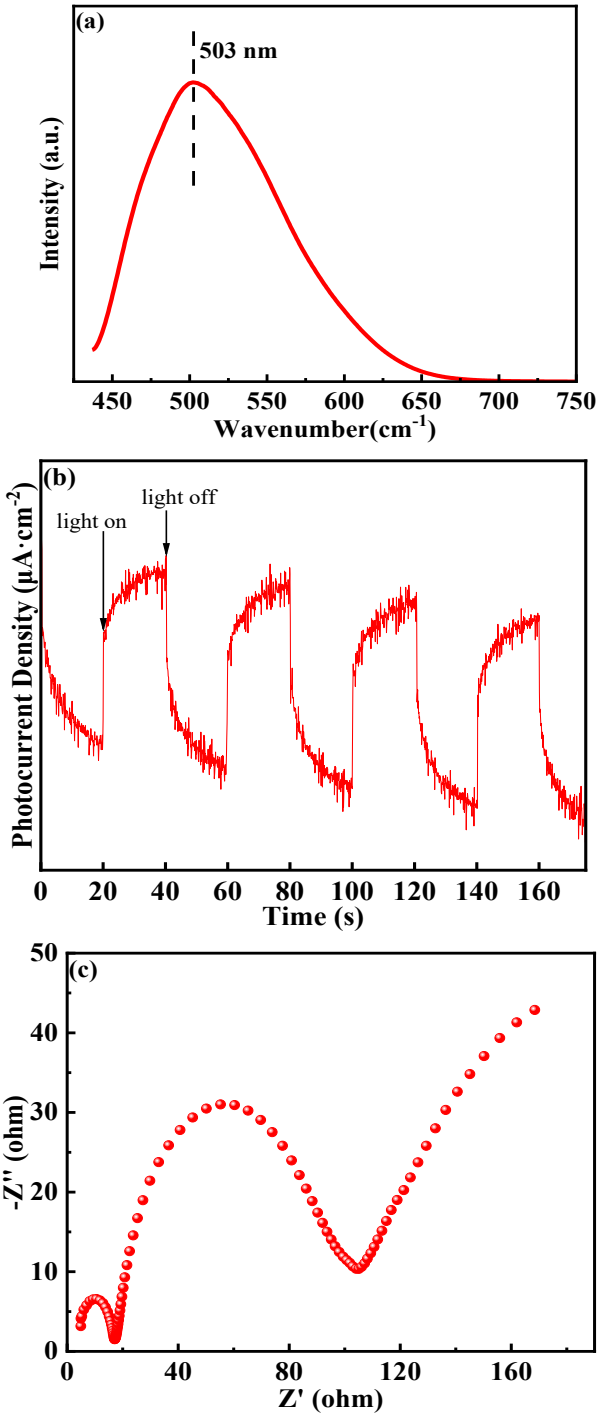

Figure 10. (a) PL spectrum, (b) transient photocurrent response, (c) Nyquist spectrum of HTCP-2.

hibiting a strong green excitation peak at 503 nm [12]. This phenomenon may be attributed to the generation of carbon quantum dots during the hydrothermal carbonization process, which adhere to the surface of carbon microspheres. The amorphous HTC material prepared by the hydrothermal method has a sp^2 hybridized structure, and the hybridized π electrons are excited by absorbing visible light photons, enabling HTC to have a broad spectral response capability.

The photocurrent and impedance tests in Figure 10(b) and 10(c) demonstrated that under visible light illumination, HTCP-2 generates photocurrent signals with photo-excited carrier generation and separation properties. However, due to sp^2 hybridization unit of HTC is in a discrete state, resulting in poor photogenerated charge transfer and conductivity performance. Therefore, HTC itself is not a well-performing and stable photocatalyst. It is shown that constructing heterojunctions by loading HTC with wide bandgap semiconductors can significantly enhance the light absorption range [37], effectively utilize the photogenerated carriers, and simultaneously leverage the synergistic effect of adsorption and photocatalysis.

4. Conclusion

Based on the perspective of efficient utilization of biomass and sustainable development, the composition, structure, and adsorption properties of hydrothermal carbons prepared from low-concentration, low-degree polymerization sugars without the use of dispersants were investigated. The experiments showed that amorphous carbon microspheres were obtained through hydrothermal carbonization at 180 °C. Increasing the glucose concentration and molecular weight of the sugar resulted in larger particle sizes of the carbon microspheres, decreased dispersibility, and an increased number of oxygen-rich nanoclusters. The surface of HTCP-2 was enriched in anionic oxygen-containing functional groups and exhibits good adsorption capacity for cationic dyes such as MB and RhB, and the adsorption process followed second-order Freundlich chemical adsorption. The synthesized HTCP demonstrated good photoelectric response capability and could be used for the preparation of adsorption-photocatalysts, providing significant potential for the synergistic treatment of pollutants through adsorption-photocatalysis.

Acknowledgments

This research was financially supported by the Natural Natural Science Foundation of China (NO. 22202169), the Science and Technology Project of Xuzhou (NO. KC21286), Innovation and entrepreneurship projects for college students (xcx2023007, xcx2023018).

Credit Author Statement

Shaojie Chen and Xinzhuo Wu: Investigation and Writing. Mei Li and Yuhan Xu: Investigation and Revision. Zihao Yuan: Investigation. Zhao Li: Revision and Funding. Jing Li: Supervision, Design, Revision & Funding.

References

[1] Liang, C.W., Fu, F.L., Tang, B. (2021). Mn-incorporated ferrihydrite for Cr(VI) immobilization: Adsorption behavior and the fate of Cr(VI) during aging. *Journal of Hazardous Materials*, 417, 126073. DOI: 10.1016/j.jhazmat.2021.126073.

[2] Wang, G.F., Hua, Y.Y., Su, X., Komarneni, S., Ma, S.J., Wang, Y.J. (2016). Cr(VI) adsorption by montmorillonite nanocomposites. *Applied Clay Science*, 124-125, 111-118. DOI: 10.1016/j.clay.2016.02.008.

[3] Cao, W., Wang, Z.Q., Ao, H.T., Yuan, B.L. (2018). Removal of Cr(VI) by corn stalk based anion exchanger: the extent and rate of Cr(VI) reduction as side reaction. *Colloids and Surfaces A: Physicochemical and Engineering Aspects*, 539, 424-432. DOI: 10.1016/j.colsurfa.2017.12.049.

[4] Zhang, L.L., An, B.H., Chen, H.J., Chu, J.J., Ma, J.X., Fan, Y.M., Wang, Z.G. (2022). Botryoidal nanolignin channel stabilized ultrasmall PdNP incorporating with filter membrane for enhanced removal of Cr(VI) via synergetic filtration and catalysis. *Separation and Purification Technology*, 296, 121409. DOI: 10.1016/j.seppur.2022.121409.

[5] Barrera-Díaz, C.E., Lugo-Lugo, V., Bilyeu, B. (2012). A review of chemical, electrochemical and biological methods for aqueous Cr(VI) reduction. *Journal of Hazardous Materials*, 223-224, 1-12. DOI: 10.1016/j.jhazmat.2012.04.054.

[6] Makama1, A.B., Salmiaton, A., Saion, E.B., Choong, T.S.Y., Abdullah, N. (2017) Photocatalytic Reduction of Aqueous Cr(VI) with CdS under Visible Light Irradiation: Effect of Particle Size. *Bulletin of Chemical Reaction Engineering & Catalysis*, 12(1), 62-70. DOI: 10.9767/bcrec.12.1.593.62-70.

[7] Ji, W., Wang, X.B., Ding, T.Q., Chakir, S., Xu, Y.F., Huang, X.H., Wang, H.T. (2022). Electrospinning preparation of nylon-6@UiO-66-NH_2 fiber membrane for selective adsorption enhanced photocatalysis reduction of Cr(VI) in water. *Chemical Engineering Journal*, 451, 138973. DOI: 10.1016/j.cej.2022.138973.

[8] Wang, J., Wang,W., Zhou S., Gao, X. (2023). Adsorption mechanism of Cr(VI) on woody-activated carbons. *Heliyon*, 9(2), e13267. DOI: 10.1016/j.heliyon.2023.e13267.

[9] Tang, J.P., Liu, Z.Y., Liu, W.F., Finfrock, Y.Z., Ye, Z.H., Liu, X., Liu, P. (2022). Application of Fe-doped biochar in Cr(VI) removal from washing wastewater and residual Cr(VI) immobilization in contaminated soil. *Journal of Cleaner Production*, 380, 134973. DOI: 10.1016/j.jclepro.2022.134973.

[10] Mallik, A.K., Moktadir, M.A., Rahman, M. A., Shahruzzaman M., Rahman Mohammed, M. (2021). Progress in surface-modified silicas for Cr(VI) adsorption: A review. *Journal of Hazardous Materials*, 423, 127041. DOI: 10.1016/j.jhazmat.2021.127041.

[11] Xi, J., Li, H., Xi, J.M., Zheng, J.L., Tan, Z.X. (2020). Preparation of high porosity biochar materials by template method: a review. *Environmental Science and Pollution Research*, 27, 20675-20684. DOI: 10.1007/s11356-020-08593-8.

[12] Yuan, J.H., Amano, Y., Machida, M. (2021). Surface characterization of mesoporous biomass activated carbon modified by thermal chemical vapor deposition and adsorptive mechanism of nitrate ions in aqueous solution. *Colloids and Surfaces A: Physicochemical and Engineering Aspects*, 616, 126213. DOI: 10.1016/j.colsurfa.2021.126213.

[13] Sewu, D.D., Woo, S.H., Lee, D.S. (2021). Biochar from the co-pyrolysis of Saccharina japonica and goethite as an adsorbent for basic blue 41 removal from aqueous solution. *Science of the Total Environment*, 797, 149160. DOI: 10.1016/j.scitotenv.2021.149160.

[14] He, Q., Yu, Y.X., Wang, J., Liu, Y.D. (2021). Kinetic study of the hydrothermal carbonization reaction of glucose and its product structure. *Industrial & Engineering Chemistry Research*, 60, 4552-4561. DOI: 10.1021/acs.iecr.0c06280.

[15] Hu, B.T., Liu, J.T., Chen, C.J., Zhao, Z., Chang, S.J., Kang, P.L. (2017). Ultra-low charge transfer resistance carbons by one-pot hydrothermal method for glucose sensing. *Science China Meterials*, 60(12): 1234-1244. DOI: 10.1007/s40843-017-9104-9.

[16] Inada, M., Enomoto, N., Hojo, J., Hayashi, K. (2016). Structural analysis and capacitive properties of carbon spheres prepared by hydrothermal carbonization. *Advanced Powder Technology*, 28, 884-889. DOI: 10.1016/j.apt.2016.12.014.

[17] Sun, Y.Y., Liu, C., Zan, Y.F., Miao, G., Wang, H., Kong, L.Z. (2018). Hydrothermal carbonization of microalgae (Chlorococcum sp.) for porous carbons with high Cr(VI) adsorption performance. *Applied Biochemistry and Biotechnology*, 186, 414–424. DOI: 10.1007/s12010-018-2752-0.

[18] Liu, Y.T., Wang, Y., Xia, H.T., Wang, Q.H., Chen, X.C., Lv, J.Q., Li, Y., Zhao, J.K., Liu, Y., Yuan, D.Z. (2022). Low-cost reed straw-derived biochar prepared by hydrothermal carbonization for the removal of uranium(VI) from aqueous solution. *Journal of Radioanalytical and Nuclear Chemistry*, 331, 3915–3925. DOI: 10.1007/s10967-022-08421-y.

[19] Hao, S.F., Zhang, Q., Wang, Y., Zhang, W.R., Huang, J.T. (2022). Preparation and adsorption properties of green sustainable biomass carbon microspheres. *Industrial & Engineering Chemistry Research*, 61: 11249-11261. DOI: 10.1021/acs.iecr.2c00094.

[20] Ibrahim, M., Hameed, B.H., Ouakouak, A., Din, A.T.M. (2022). Effect of hydrothermal carbonization parameters and performance of carbon dioxide adsorption on pineapple peel waste biochar. *Chemical Engineering & Technology*, 45, 1982-1989. DOI: 10.1002/ceat.202200089.

[21] Xu, D.Y., Sun, T., Jia, H.T., Sun, Y.B., Zhu, X.P. (2022). The performance and mechanism of Cr(VI) adsorption by biochar derived from potamogeton crispus at different pyrolysis temperatures. *Journal of Analytical and Applied Pyrolysis*, 167, 105662. DOI: 10.1016/j.jaap.2022.105662.

[22] Cai, W.Q., Wei, J.H., Li, Z.L., Liu, Y., Zhou, J.B., Han, B. (2019). Preparation of amino-functionalized magnetic biochar with excellent adsorption performance for Cr(VI) by a mild one-step hydrothermal method from peanut hull. *Colloids and Surfaces A: Physicochemical and Engineering Aspects*, 563, 102-111. DOI: 10.1016/j.colsurfa.2018.11.062.

[23] Sheng, K.C., Zhang, S., Liu, J.L., E, S., Jin, C.D., Xu, Z.H., Zhang, X.M. (2019). Hydrothermal carbonization of cellulose and xylan into hydrochars and application on glucose isomerization. *Journal of Cleaner Production*, 237, 117831. DOI: 10.1016/j.jclepro.2019.117831.

[24] Wu, J., Yang, J.W., Huang, G.H., Xu, C.H., Lin, B.F. (2019). Hydrothermal carbonization synthesis of cassava slag biochar with excellent adsorption performance for Rhodamine B. *Journal of Cleaner Production*, 251, 119717. DOI: 10.1016/j.jclepro.2019.119717.

[25] Jian, X.M., Zhuang, X.Z., Li, B.S., Xu, X.W., Wei, Z.B., Song, Y.P., Jiang, E.C. (2018). Comparison of characterization and adsorption of biochars produced from hydrothermal carbonization and pyrolysis. *Environmental Technology & Innovation*, 10, 27-35. DOI: 10.1016/j.eti.2018.01.004.

[26] Jung, D., Kruse, A., Duman, G., Yanik, J., Zimmermann, M. (2021). Hydrothermal carbonization of fructose—effect of salts and reactor stirring on the growth and formation of carbon spheres. *Biomass Conversion and Biorefinery*, 13, 6281-6297. DOI: 10.1007/s13399-021-01782-6.

[27] Wortmann, M., Keil, W., Diestelhorst, E., Westphal, M., Haverkamp, R., Brockhagen, B., Biedinger, J., Bondzio, L., Wwinberger, C., Baier, D., Tiemann, M., Hütten, A., Hellweg, T., Reiss, G., Schmidt, C., Sattler, K., Frese, N. (2023). Hard carbon microspheres with bimodal size distribution and hierarchical porosity via hydrothermal carbonization of trehalose. *RSC Advances*, 13: 14181-14189. DOI: 10.1039/d3ra01301d.

[28] Ischia, G., Cutillo, M., Guella, G., Bazzanella, N., Cazzanelli, M., Orlandi, M., Miotello, A., Fiori, L. (2022). Hydrothermal carbonization of glucose: Secondary char properties, reaction pathways, and kinetics. *Chemical Engineering Journal*, 449, 137827. DOI: 10.1016/j.cej.2022.137827.

[29] Liu, J., Tian, P., Ye, J.W., Zhou, L., Gong, W.T., Lin, Y., Ning, G.L. (2009). Hydrothermal synthesis of carbon microspheres from glucose: Tuning sphere size by adding oxalic acid. *Chemistry Letters*, 38(10), 948-949. DOI: 10.1246/cl.2009.948.

[30] Yao, Z.Y., Zhang, W.Q., Yu, X.Y. (2023). Fabricating porous carbon materials by one-step hydrothermal carbonization of glucose. *Processes*, 11(7), 1923. DOI: 10.3390/pr11071923.

[31] Li, M., Li, W., Liu, S.X. (2012). Control of the morphology and chemical properties of carbon spheres prepared from glucose by a hydrothermal method. *Journal of Materials Research*, 27, 1117-1123. DOI: 10.1557/jmr.2011.44.

[32] Tovar-Martinez, E., Sanchez-Rodriguez, C.E., Sanchez-Vasquez, J.D., Reyes-Reyes, M., López-Sandoval, R. (2023). Synthesis of carbon spheres from glucose using the hydrothermal carbonization method for the fabrication of EDLCs. *Diamond and Related Materials*, 136, 110010. DOI: 10.1016/j.diamond.2023.110010.

[33] Song, X., Mo, J., Fang, Y., Luo, S., Xu, J., Wang, X. (2022). Synthesis of magnetic nanocomposite Fe3O4@ZIF-8@ZIF-67 and removal of tetracycline in water. *Environmental Science and Pollution Research*, 29, 35204–35216. DOI: 10.1007/s11356-021-18042-9.

[34] Liu, Y., Wang, Y., Xia, H., Wang, Q., Chen, X., Lv, J., Li, Y., Zhao, J., Liu, Y., Yuan, D. (2022). Low-cost reed straw-derived biochar prepared by hydrothermal carbonization for the removal of uranium(VI) from aqueous solution. *Journal of Radioanalytical and Nuclear Chemistry*, 331, 3915–3925. DOI: 10.1007/s10967-022-08421-y.

[35] Cao, Y., Wu, X., Li, B., Tang, X., Lin, X., Li, P., Chen, H., Huang, F., Wei, C., Wei, J., Qiu, G. (2023). Ca–La layered double hydroxide (LDH) for selective and efficient removal of phosphate from wastewater. *Chemosphere*, 325, 138378. DOI: 10.1016/j.chemosphere.2023.138378.

[36] Zhu, Y., Ji, H., He, K., Blaney, L., Xu, T., Zhao, D. (2022). Photocatalytic degradation of GenX in water using a new adsorptive photocatalyst. *Water Research*, 220, 118650. DOI: 10.1016/j.watres.2022.118650.

[37] Cheng, S., Zhao, S.D., Xing, B.L., Liu, Y.Z., Zhang, C.X., Xia, H.Y. (2022). Preparation of magnetic adsorbent-photocatalyst composites for dye removal by synergistic effect of adsorption and photocatalysis. *Journal of Cleaner Production*, 348, 131301. DOI: 10.1016/j.jclepro.2022.131301.